Many-body localization and mobility edge in a disordered spin-$\frac{1}{2}$ Heisenberg ladder

Elliott Baygan, S. P. Lim, and D. N. Sheng
Department of Physics and Astronomy, California State University, Northridge, California 91330, USA
(Received 28 September 2015; revised manuscript received 10 November 2015; published 30 November 2015)

We examine the interplay of interaction and disorder for a Heisenberg spin-1/2 ladder system with random fields. We identify many-body localized states based on the entanglement entropy scaling, where delocalized and localized states have volume and area laws, respectively. We first establish the dynamic phase transition at a critical random field strength $h_c \sim 8.5 \pm 0.5$, where all energy eigenstates are localized beyond that value. Interestingly, the entanglement entropy and fluctuations of the bipartite magnetization show distinct probability distributions which characterize different phases. Furthermore, we show that for weaker h, energy eigenstates with higher-energy density are delocalized while states at lower-energy density are localized, which defines a mobility edge separating these two phases. With increasing disorder strength, the mobility edge moves towards higher-energy density, which drives the system to the phase of the full many-body localization.

DOI: 10.1103/PhysRevB.92.195153 PACS number(s): 75.10.Pq, 71.30.+h, 73.22.Gk

I. INTRODUCTION

Anderson localization theory [1] predicts that noninteracting electrons are generally localized in one- and two-dimensional (1D and 2D) disordered systems without either a magnetic field or spin-orbit coupling due to destructive quantum interference. It is generally believed that low-energy states remain localized for weakly interacting systems [2–7] with characteristic features different from noninteracting systems. Recently, there has been renewed interest to examine the Anderson localization for interacting systems, where the phenomenon of many-body localization (MBL) [8,9] has attracted intense study. Many remarkable properties of an MBL phase have been established [8–49] based on combined theoretical and numerical studies. For disordered interacting systems, the random disorder can drive a dynamic phase transition [8,22,50] from a delocalized state to an MBL phase, where energy eigenstates at finite energy density become localized. From the quantum information perspective, energy eigenstates in an MBL phase have suppressed entanglement entropy satisfying an area law [8,17,26,36] scaling with the subsystems boundary area in contrast to the volume-law scaling expected for an ergodic delocalized state. As a consequence, the MBL phase is nonergodic and cannot thermalize [11,51,52], which also challenges the fundamental "eigenstate thermalization hypothesis" (ETH) for quantum statistical physics [53]. The MBL state may exhibit quantum order or topological order [16,36,43,54–58] at finite temperature as excitations at finite energy density are localized. A phenomenological study [14] further establishes that the MBL phase behaves like integrable systems, respecting extensive numbers of local conservation laws [15,20,59]. The phase transition from an MBL phase to a delocalized ergodic phase may be continuous, characterized by a jump of the entanglement entropy in the thermodynamic limit [17], where both entropy and its variance grow with the system volume at the critical point [14,26]. Interestingly, it is conjectured that an MBL phase can also have a continuous localization-delocalization transition to a new state, where the delocalized phase is nonergodic whose volume-law entanglement entropy tends to zero as the transition is approached [17]. It may be possible to have the MBL phase in multicomponent systems without random disorder [60,61]. The MBL phase may be detected experimentally in cold-atom systems [12,13,18,19,62].

So far, much of the quantitative understanding of MBL systems is based on numerical exact-diagonalization (ED) studies [12,19,21–36,63] of spin and electron systems, where the dynamic phase transition between a delocalization phase and an MBL phase has been demonstrated for different 1D model systems with spin (or particle) numbers in the range $N = 10$–22 [26,46]. There are also some recent developments [64–69] using tensor network and density matrix renormalization-group approaches to study such systems. One of the conceptually important and unsettled issues is whether the mobility edge exists for the microscopic system to separate the low-energy localized state from the higher-energy extended states. On the one hand, these ED studies [26,46] have demonstrated the energy density dependence of the critical random field, consistent with the existence of the mobility edge. In particular, Luitz *et al.* [46] studied the 1D spin-1/2 Heisenberg chain in a random field using the shift-inverted spectral transformation method dealing with up to 22 spins, where the finite-size scaling has been demonstrated with convincing accuracy, supporting the existence of the mobility edge. However, the recent numerical linked cluster expansion study [70] for a thermodynamic system finds that a higher disorder strength (as the lower bound) is required to enter the MBL phase than that obtained by ED studies. The reason for such a discrepancy is still not understood. On the theoretical side, it is not clear [32,44,71–73] if some spatial region with higher-energy density may play an important role with more extensive wave functions, which may melt the lower-energy eigenstates in the system into delocalized states with increasing the system size. Some insight on this issue may come from the earlier study of interacting many-body systems with random disorder [74–76], which exhibit the fractionalized quantum Hall effect. In such a system, we have demonstrated that low-energy states below a mobility edge have topological order protected by a mobility gap which separates the low-energy localized insulating states from the metallic states above the mobility edge. These earlier studies suggest that it is possible to follow the evolution of the low-energy eigenstates in disordered interacting systems to detect if the mobility edge generally exists for MBL systems.

In this paper, we numerically examine the interplay of interaction and random disorder field for two-leg spin-1/2 Heisenberg ladder systems, which stands between 1D and 2D systems [40,62], with the latter being much harder to be systematically studied based on the ED method. We identify MBL states based on the bipartite entanglement entropy scaling, and the spectral statistics of many-body energy levels. We first establish the phase transition at a critical random field strength $h_c \sim 8.5 \pm 0.5$, where all energy eigenstates are localized beyond that value. Interestingly, the entanglement entropy shows distinct probability distribution in different phases, while the transition is associated with the fast growing of the variance for the entropy with the increase of the system size N [26,46]. Despite the small system sizes that we can access with the number of spins $N = 12$–20, our entropy distribution matches the theoretic prediction [71] in both the delocalized phase and MBL phase, indicating that we were able to access universal characteristics of these different phases. Furthermore, we show that at weaker h, energy eigenstates with higher-energy density are delocalized while states at lower density are localized, which defines a mobility edge separating these two dynamically distinct phases, in agreement with earlier results for 1D spin chain systems [26,46]. Using the energy-resolved entanglement entropy, we observe that the mobility edge moves to higher-energy density with the increase of the random field strength, which eventually drives the system to the phase with full MBL where all energy eigenstates are localized.

The remainder of the paper is organized as follows: In Sec. II, we first introduce the two-leg ladder spin-1/2 model with random fields and briefly discuss the method we use to study the system. We present the evidence of the MBL phase determined by the entanglement entropy, fluctuations of the half-system magnetization, and the energy level statistics studies. In Sec. III, we study the characteristic features of different phases and the transition between the delocalized phase and the MBL phase. We also present the evidence for the mobility edge separating the low-energy localized phase from the higher-energy extended states. Finally, in Sec. IV, we summarize our main results and discuss open questions.

II. SPIN MODEL AND TRANSITION TO AN MBL PHASE

We study the spin-1/2 Heisenberg two-leg ladder system on the square lattice with the following Hamiltonian:

$$H = J \sum_{\langle i,j \rangle} \vec{S}_i \cdot \vec{S}_j - \sum_i h_i S_i^z,$$

where the summation $\langle i,j \rangle$ runs over all distinct nearest-neighbor bonds with antiferromagnetic coupling J, which is set as the units of the energy $J = 1$. The h_i is a random magnetic field coupling, which distributes uniformly between window $(-h,h)$, with h as the strength of random fields. The number of sites of the ladder system can be written as $N = N_x N_y$, with $N_y = 2$ and N_x the number of sites along each spin chain.

We perform Lanczos ED calculations to obtain energy eigenstates around a fixed value E determined by the target energy density ε (which is the normalized dimensionless energy) for systems with the number of sites $N = 12$–20 in the total $S^z = 0$ sector. Specifically, for each disorder configuration, we first calculate the ground-state energy E_0 and the maximum energy $E_{\max}$, which are used to define the target energy density $\varepsilon = (E - E_0)/(E_{\max} - E_0)$. Physical quantities [46] at finite energy density including the bipartite entanglement entropy, energy level statistics, and bipartite fluctuations of the subsystem magnetization are obtained and averaged over more than 1000 disorder configurations and 30 energy eigenstates from each configuration near the given energy density ε. For mobility edge simulations [see Figs. 4(a) and 4(b)], we follow up to 360 lowest-energy eigenstates, and obtain entanglement entropies for each of these eigenstates by performing 1000 disorder configuration averages.

The bipartite entanglement entropy has been extensively used as an effective tool to characterize many-body phases for such an interacting system [8,26,46]. We compute the von Neumann entanglement entropy of the ladder system from all eigenvalues of the reduced density matrix ρ_A as $S = -\mathrm{Tr}\rho_A \ln \rho_A$, by partitioning the system in the middle along the vertical direction [the lengths for two subsystems A and B are the integer parts of $N_x/2$ and $(N_x + 1)/2$, respectively]. For an interacting system with weak disorder, the entanglement entropies of higher-energy eigenstates are expected to follow the volume law and these states are ergodic satisfying the ETH [8,9]. This is in contrast to the behavior of the ground state, where the entanglement entropy follows the area law (with possibly up to the logarithmic correction depending on whether there are gapless excitations) [17]. By varying the disorder strength h, one can detect the possible phase transition from the behavior of the entanglement entropy [26,46]. As shown in Fig. 1(a), we plot the ratio of entanglement entropy over the number of system sites S/N for different systems from $N_x = 6$ to 9 at the energy density $\varepsilon = 0.5$ as a function of random field strength h. On the smaller-h side, we see that the ratio S/N increases with system sizes N and approaches a constant, indicating the volume-law growth of S. With varying h, all data points approximately cross each other around a critical value $h_c \sim 8.5 \pm 0.5$. On the larger-h side, S/N approaches zero, indicating the low entanglement and nonergodic behavior where energy eigenstates are localized. The ladder systems that we study here have a stronger finite-size effect (from the even-odd effect of N_x) than the 1D spin chain systems, which is the reason that not all curves cross at the same point in Fig. 1(a).

We further use the level statistics analysis from the random matrix theory [21,77] to probe the localization-delocalization characteristics of energy eigenstates. In the delocalized regime, the level-spacing distribution is described by the Gaussian orthogonal ensemble (GOE) statistics, which represents extended levels with level repulsion between them because of the overlap of energy eigenstates in real space. In the localized regime, the level-spacing distribution is determined by Poisson statistics as wave functions close in energy are exponentially localized with no level repulsion between them [78]. In the energy spectrum analysis [46], we define the energy gap $\delta_n = E_n - E_{n-1}$ as the energy difference between the nth and $(n-1)$th eigenstates; then the adjacent gap ratio can be defined as $r_n = \min(\delta_n, \delta_{n+1})/\max(\delta_n, \delta_{n+1})$. We average the gap ratio $r = \langle r_n \rangle$ over states near the spectrum center at $\varepsilon = 0.5$ for 30 eigenstates from each disorder configuration and 1000

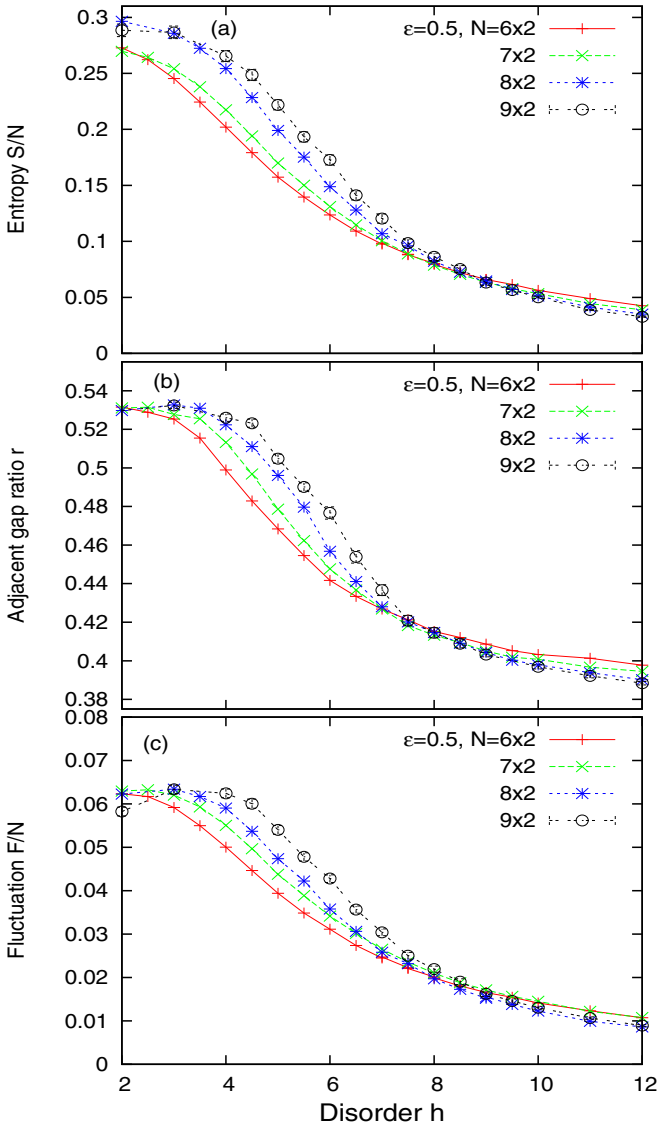

FIG. 1. (Color online) (a) The ratio of entanglement entropy over the number of system sites S/N for different systems from $N = 6 \times 2$ to 9×2 at the energy density $\varepsilon = 0.5$ as a function of random disorder strength h. Curves for different N approximately cross each other around a critical $h_c = 8.5 \pm 0.5$. (b) The adjacent gap ratio r for states with energy density $\varepsilon = 0.5$ as a function of h. Here we see that on the small-h side, r approaches the Gaussian orthogonal ensemble value (0.5307) representing delocalized states, while at the larger-h side, r reaches the Poisson value ($2\ln 2 - 1 \simeq 0.3863$) for larger systems representing localized states. All curves cross around the critical value $h_c = 8.0 \pm 0.5$. (c) The ratio of the fluctuations of half-system magnetization over the number of system sites F/N as a function of h. Curves for even (odd) N_x approximately cross each other around $h_c \sim 8$–9. The standard error bars for the largest system $N = 18$ are shown in (a)–(c), while other data for smaller N have smaller error bars. Combining the above results, we estimate the critical point is around $h_c = 8.5 \pm 0.5$.

random disorder configurations for each disorder strength h. As shown in Fig. 1(b), we see that at the small-h side, r approaches the Gaussian orthogonal ensemble value (0.5307) representing delocalized states, while at the stronger h side, r reaches the Poisson value ($2\ln 2 - 1 \simeq 0.3863$) for larger systems representing the level statistics of localized states. All curves cross around the critical value $h_c \sim 8.0$–8.5.

We compare the entanglement entropy behavior with the bipartite fluctuations F of the subsystem magnetization S_A^z [46,79], which is defined as $F = \langle (S_A^z)^2 \rangle - \langle S_A^z \rangle^2$ as shown in Fig. 1(c). We plot the ratio F/N for different systems from $N_x = 6$ to 9 at the energy density $\varepsilon = 0.5$ as a function of random field strength h. On the smaller-h side, we see that F/N increases with system sizes N and approaches a constant, indicating the volume-law growth of F. On the larger-h side, F/N approaches zero, indicating the low fluctuations where energy eigenstates are localized. However, comparing curves with different N, we observe a larger finite-size effect for F (from the even-odd effect of N_x). This is due to the fact that the half-system partition for odd N_x will cut through a vertical bond, which gives rise to larger F at the larger-h side. Combining results from Figs. 1(a)–1(c), we find that the ergodic behavior is established around the $h < 8$ side, while the MBL phase is robust at the $h > 9$ side, which leads to the estimate of the critical point for the dynamic phase transition $h_c = 8.5 \pm 0.5$. Due to the stronger finite-size effect here and the small range of $N_x = 6$–9, we do not attempt to do a finite-size scaling. Instead, we will focus on the general behavior of the different phases to explore characteristic features of the phases and the transition involved here.

III. CHARACTERISTIC FEATURES OF DIFFERENT PHASES AND PHASE TRANSITION

A. Probability distributions of entanglement entropy and variance of bipartite magnetization

Now we turn to the study of the probability density distribution of the entropy $P(S)$ for a spin system at energy density $\varepsilon = 0.5$ for different disorder strengths $h = 4$, 6, 8, and 10 crossing two different phases obtained for ensembles with 30 energy eigenstates (for each disorder configuration) and 1000 disorder configurations for each h. As shown in Fig. 2(a), on the small-h side, we see that the peak position of the distribution $P(S)$ (which reflects the average of S) moves to the larger-S value with increasing system size N, indicating a consistency with the volume law for the entropy. Close to the transition point for $h = 6$, we find that the distribution $P(S)$ becomes much broadened while the peak position moves to the higher S with the increase of N, but the peak height reduces at the same time. As we move to the higher-h side, we see that the distribution again becomes sharper, with two peaks showing for each $P(S)$ curve, which may be related to the nonergodic character of the localized phase. The second peak is located at the entropy value $S = \ln 2$, indicating the contribution of the locally entangled spin pairs. Furthermore, we also see that for the stronger disorder case, the distribution always has a long tail into higher-S values, while for smaller h, the long tail is at the smaller-S side. To compare with the recent theoretical description of the MBL of a 1D system [71], we find that the entropy distribution is very similar to the ones obtained based on their real-space renormalization-group simulations. Specifically, at $h = 4$, our distribution has a long tail in the small-S region for our finite-size results, which indicates the

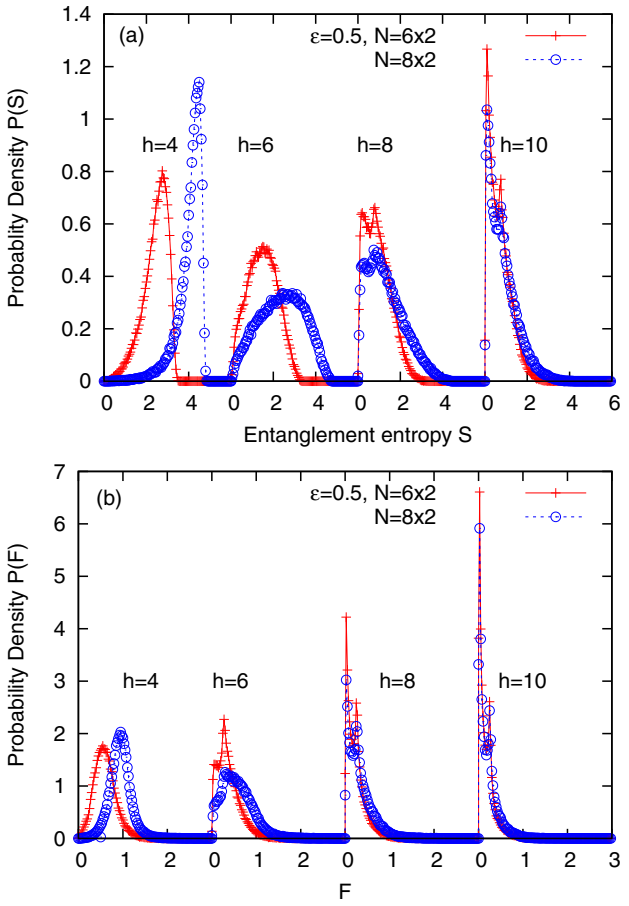

FIG. 2. (Color online) (a) The probability density distributions of the bipartition entanglement entropy $P(S)$ for spin system at energy density $\varepsilon = 0.5$ with different disorder strengths $h = 4$, 6, 8, and 10 for $N = 6 \times 2$ and 8×2. These results illustrate that for a stronger disorder case, the distribution always has a long tail into higher-S values, while for smaller h, the long tail is on the small-S side. (b) The probability distributions $P(F)$ of the variance $F = \langle (S_A^z)^2 \rangle - \langle S_A^z \rangle^2$ (in units of the square of the Planck constant $\hbar^2$) of the magnetization of the half system A for spin system at energy density $\varepsilon = 0.5$ with different disorder strengths $h = 4$, 6, 8, and 10 for $N = 6 \times 2$ and 8×2. Error bars for all data points in (a) and (b) are comparable to the size of the symbols.

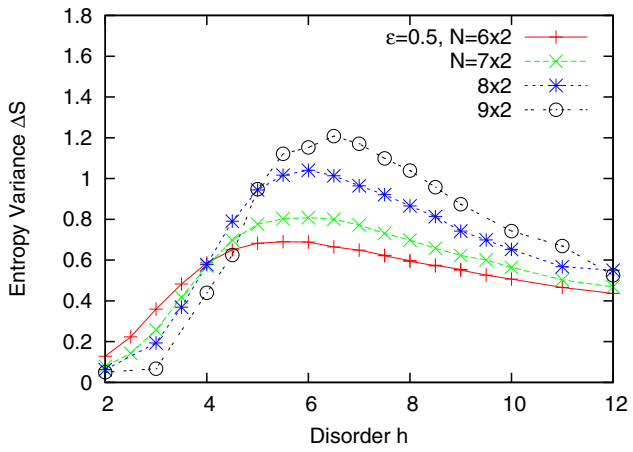

FIG. 3. (Color online) (a) The variance $(\Delta S)^2 = \langle S^2 \rangle - \langle S \rangle^2$ of the entanglement entropy at energy density $\varepsilon = 0.5$ for different h. ΔS reaches the peak value at h_p smaller than the identified h_c for phase transition. Clearly, h_p shifts to higher h with the increase of N. The error bars are comparable to the size of the symbols.

remaining localized states (regions) inside the ergodic phase. However, with the increase of N, the physics will be dominated by states with larger S and the distribution will become a δ function. At $h = 10$, we find that the $P(S)$ is peaked at $S = 0$ and shows an exponential decay tail on the larger-S side. Furthermore, the $P(S)$ shows weak N dependence, which will remain broad in the thermodynamic limit characterizing the MBL phase.

We compare the entanglement entropy behavior with the bipartite fluctuations F of the subsystem magnetization, as shown in Fig. 2(b). The distribution $P(F)$ exhibits very similar behavior as $P(S)$ for h closer to the phase transition and in the MBL phase. The similar two-peak structure is also clear for $P(F)$ on the larger-h side in the MBL phase. The only difference worth mentioning is that with weaker disorder $h = 4$, the $P(F)$ demonstrates the normal Gaussian distribution, which is sharp and near symmetric about the peak.

The variance of the entanglement entropy has been shown to be an excellent quantity [26,71] for identifying the phase transition from 1D spin chain studies. Here we show the variance ΔS of the entanglement entropy averaged over 1000 disorder configurations and 30 different energy eigenstates from each configuration around the energy density $\varepsilon = 0.5$. In agreement with these observations for 1D systems [26,46], we find that the ΔS is small in both small-h and large-h sides, and demonstrates a peak for the intermediate h, as shown in Fig. 3. We observe that the peak value of ΔS increases with N, which may diverge at the transition point. The position of the peak h_p is smaller than the previously identified h_c and it shows a trend of approaching h_c with the increase of N. These results are consistent with the phenomenological theory [71] established based on the real-space renormalization-group studies, which indicate that we are observing intrinsic properties of the MBL phase and the related phase transition for the system sizes that we study. We comment that for the given range of system sizes that we can access, one cannot make a definite conclusion as to whether there is an intermediate regime where the variance of the entropy may diverge in the thermodynamic limit.

B. Possible existence of mobility edge

We have shown that the disorder can drive a phase transition where all states near the center of the energy spectrum are localized. In fact, all other states with different energy density are also localized, and thus we enter the full MBL phase tuned by h [see Fig. 4(c) as an example]. To address the issue of whether the mobility edge naturally exists at the smaller $h < h_c$ side in such a system, separating low-energy MBL states from higher-energy delocalized ergodic states, we obtain up to 360 lowest eigenstates using Lanczos ED. We follow the entropy of each energy eigenstate S_i in the lower-energy density regime and average that over 1000 disorder configurations.

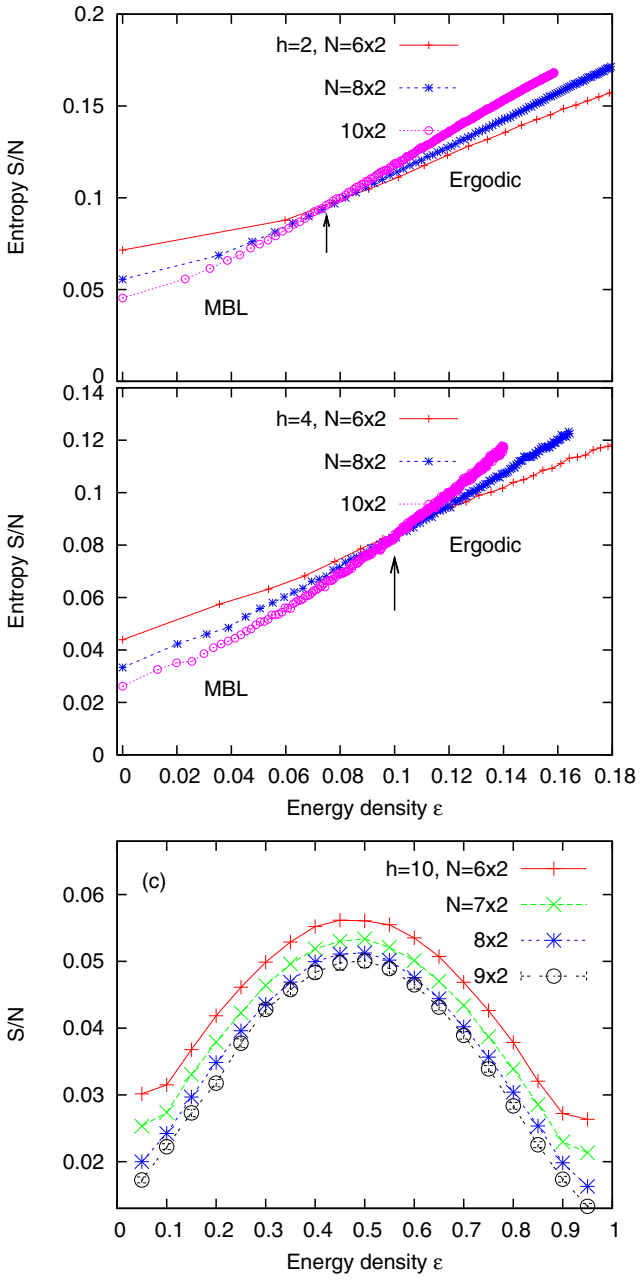

FIG. 4. (Color online) The entropy of each energy eigenstate S_i for low-energy eigenstates averaged over disorder configurations is shown as a function of its average energy density. S_i/N curves for different system sizes $N = 6 \times 2, 8 \times 2$, and 10×2 cross at a critical energy density ε_c, which separates the higher-energy delocalized ergodic states from the lower-energy MBL states. The error bars for the $N = 18$ system in (c) are shown, while all other data in (a)–(c) have a typical error bar that is smaller than or around the same size as the symbols.

As shown in Figs. 4(a) and 4(b) for $h = 2$ and 4, we identify that the disorder configuration averaged entropy S_i for the ith energy eigenstate is a smoothly increasing function of eigenenergy E_i or its average energy density $\varepsilon_i = \langle (E_i - E_0)/(E_{\max} - E_0) \rangle$. The entropy per site S_i/N for different system sizes $N = 6 \times 2, 8 \times 2$, and 10×2 crosses around a critical energy density ε_c, which separates higher-energy states with volume-law entropy (ergodic delocalized states) from lower-energy localized states with S_i/N approaching zero, violating the volume law. Here all of the data we show have even $N_x = 6$, 8, and 10 with reduced finite-size effect. The crossing point determines the mobility edge. With increasing h, the entropy of the low-lying eigenstate is reduced and the mobility edge is being pushed to the higher-energy density from $\varepsilon_c \sim 0.075$ at $h = 2$ to $\varepsilon_c \sim 0.1$ at $h = 4$. We comment that much larger system study by DMRG method [64,65,80] is required to fully determine the scaling of the mobility edge. As shown in Fig. 4(c), we further move to the stronger disorder case, at $h = 10$, and we see that S/N at different energy density (here we averaged over both disorder configurations and energy eigenstates for each energy density ε) is always a decreasing function with increasing N, demonstrating that all states are localized.

IV. SUMMARY AND DISCUSSION

We have identified the disorder-driven dynamic phase transition from an ergodic delocalized phase to an MBL nonergodic phase for two-leg ladder Heisenberg spin-1/2 systems with random field disorder. The characteristic distributions of the entanglement entropy for both the delocalized phase and the MBL phase agree with the theoretical description for the MBL [71]. Furthermore, we show that for weaker h, energy eigenstates with higher-energy density are delocalized while states at lower density are localized, which defines a mobility edge separating these two dynamically distinct quantum states, in agreement with earlier results for 1D spin chain systems [26,46]. On the quantitative side, we find that the Heisenberg ladder requires a much higher critical disorder strength $h_c \sim 8.5 \pm 0.5$ compared to the 1D spin chain model ($h_c \sim 3.5$) [46] to enter the full MBL phase. It is crucial to study multileg ladders for such systems to determine if the MBL phase has very strong critical disorder strength h_c or even divergent h_c in the 2D limit, which we leave for a future study.

ACKNOWLEDGMENTS

We thank Tarun Grover and David Huse for stimulating discussions. This work is supported by the U.S. National Science Foundation Grants No. PREM DMR-1205734 (EB), No. DMR-1408560, and Princeton MRSEC Grant No. DMR-1420541 for travel support.

[1] P. W. Anderson, Phys. Rev. **109**, 1492 (1958).
[2] D. M. Basko, I. L. Aleiner, and B. L. Altshuler, Ann. Phys. (NY) **321**, 1126 (2006).
[3] L. Fleishman and P. W. Anderson, Phys. Rev. B **21**, 2366 (1980).
[4] B. L. Altshuler, Y. Gefen, A. Kamenev, and L. S. Levitov, Phys. Rev. Lett. **78**, 2803 (1997).
[5] P. Jacquod and D. L. Shepelyansky, Phys. Rev. Lett. **79**, 1837 (1997).

[6] B. Georgeot and D. L. Shepelyansky, Phys. Rev. Lett. **81**, 5129 (1998).
[7] I. V. Gornyi, A. D. Mirlin, and D. G. Polyakov, Phys. Rev. Lett. **95**, 206603 (2005).
[8] R. Nandkishore and D. A. Huse, Annu. Rev. Cond. Matt. Phys. **6**, 15 (2015).
[9] E. Altman and R. Vosk, Annu. Rev. Cond. Matt. Phys. **6**, 383 (2015).
[10] R. Nandkishore, S. Gopalakrishnan, and D. A. Huse, Phys. Rev. B **90**, 064203 (2014).
[11] M. Rigol, V. Dunjko, and M. Olshanii, Nature (London) **452**, 854 (2008).
[12] M. Serbyn, M. Knap, S. Gopalakrishnan, Z. Papić, N. Y. Yao, C. R. Laumann, D. A. Abanin, M. D. Lukin, and E. A. Demler, Phys. Rev. Lett. **113**, 147204 (2014).
[13] M. P. Kwasigroch and N. R. Cooper, Phys. Rev. A **90**, 021605 (2014).
[14] D. A. Huse, R. Nandkishore, and V. Oganesyan, Phys. Rev. B **90**, 174202 (2014).
[15] M. Serbyn, Z. Papić, and D. A. Abanin, Phys. Rev. Lett. **111**, 127201 (2013).
[16] A. Chandran, V. Khemani, C. R. Laumann, and S. L. Sondhi, Phys. Rev. B **89**, 144201 (2014).
[17] T. Grover, arXiv:1405.1471.
[18] N. Y. Yao, C. R. Laumann, S. Gopalakrishnan, M. Knap, M. Müller, E. A. Demler, and M. D. Lukin, Phys. Rev. Lett. **113**, 243002 (2014).
[19] R. Vasseur, S. A. Parameswaran, and J. E. Moore, Phys. Rev. B **91**, 140202 (2015).
[20] V. Ros, M. Müller, and A. Scardicchio, Nucl. Phys. B **891**, 420 (2015).
[21] V. Oganesyan and D. A. Huse, Phys. Rev. B **75**, 155111 (2007).
[22] A. Pal and D. A. Huse, Phys. Rev. B **82**, 174411 (2010).
[23] M. Žnidarič, T. Prosen, and P. Prelovšek, Phys. Rev. B **77**, 064426 (2008).
[24] E. Canovi, D. Rossini, R. Fazio, G. E. Santoro, and A. Silva, Phys. Rev. B **83**, 094431 (2011).
[25] E. Cuevas, M. Feigel'Man, L. Ioffe, and M. Mezard, Nat. Commun. **3**, 1128 (2012).
[26] J. A. Kjäll, J. H. Bardarson, and F. Pollmann, Phys. Rev. Lett. **113**, 107204 (2014).
[27] A. De Luca and A. Scardicchio, Europhys. Lett. **101**, 37003 (2013).
[28] S. Iyer, V. Oganesyan, G. Refael, and D. A. Huse, Phys. Rev. B **87**, 134202 (2013).
[29] S. Johri, R. Nandkishore, and R. N. Bhatt, Phys. Rev. Lett. **114**, 117401 (2015).
[30] J. H. Bardarson, F. Pollmann, and J. E. Moore, Phys. Rev. Lett. **109**, 017202 (2012).
[31] F. Andraschko, T. Enss, and J. Sirker, Phys. Rev. Lett. **113**, 217201 (2014).
[32] C. R. Laumann, A. Pal, and A. Scardicchio, Phys. Rev. Lett. **113**, 200405 (2014).
[33] J. M. Hickey, S. Genway, and J. P. Garrahan, arXiv:1405.5780.
[34] A. Nanduri, H. Kim, and D. A. Huse, Phys. Rev. B **90**, 064201 (2014).
[35] Y. Bar Lev and D. R. Reichman, Phys. Rev. B **89**, 220201 (2014).
[36] B. Bauer and C. Nayak, J. Stat. Mech. Theor. Expt. (2013) P09005.
[37] J. Z. Imbrie, arXiv:1403.7837.
[38] M. Serbyn and J. E. Moore, arXiv:1508.07293.
[39] R. Singh, J. H. Bardarson, and F. Pollmann, arXiv:1508.05045.
[40] Y. Bar Lev and D. R. Reichman, arXiv:1508.05391.
[41] D.-L. Deng, J. H. Pixley, X. Li, and S. Das Sarma, arXiv:1508.01270.
[42] X. Chen, X. Yu, G. Y. Cho, B. K. Clark, and E. Fradkin, arXiv:1509.03890.
[43] D. Pekker, G. Refael, E. Altman, E. Demler, and V. Oganesyan, Phys. Rev. X **4**, 011052 (2014).
[44] Y. Huang, arXiv:1507.01304.
[45] Y.-Z. You, X.-L. Qi, and C. Xu, arXiv:1508.03635.
[46] D. J. Luitz, N. Laflorencie, and F. Alet, Phys. Rev. B **91**, 081103 (2015).
[47] K. Agarwal, S. Gopalakrishnan, M. Knap, M. Müller, and E. Demler, Phys. Rev. Lett. **114**, 160401 (2015).
[48] S. Gopalakrishnan, M. Mueller, V. Khemani, M. Knap, E. Demler, and D. A. Huse, Phys. Rev. B **92**, 104202 (2015).
[49] X. Li, S. Ganeshan, J. H. Pixley, and S. Das Sarma, Phys. Rev. Lett. **115**, 186601 (2015).
[50] A. C. Potter, R. Vasseur, and S. A. Parameswaran, Phys. Rev. X **5**, 031033 (2015).
[51] J. M. Deutsch, Phys. Rev. A **43**, 2046 (1991).
[52] M. Srednicki, Phys. Rev. E **50**, 888 (1994).
[53] P. Hosur and X.-L. Qi, arXiv:1507.04003.
[54] D. A. Huse, R. Nandkishore, V. Oganesyan, A. Pal, and S. L. Sondhi, Phys. Rev. B **88**, 014206 (2013).
[55] Y. Bahri, R. Vosk, E. Altman, and A. Vishwanath (unpublished).
[56] R. Vosk and E. Altman, Phys. Rev. Lett. **112**, 217204 (2014).
[57] A. C. Potter and A. Vishwanath, arXiv:1506.00592.
[58] N. Y. Yao, C. R. Laumann, and A. Vishwanath, arXiv:1508.06995.
[59] A. Chandran, J. Carrasquilla, I. H. Kim, D. A. Abanin, and G. Vidal, Phys. Rev. B **92**, 024201 (2015).
[60] P. Ponte, Z. Papić, F. Huveneers, and D. A. Abanin, Phys. Rev. Lett. **114**, 140401 (2015).
[61] T. Grover and M. P. A. Fisher, J. Stat. Mech. Theor. Expt. (2014) P10010.
[62] P. Bordia, H. P. Lüschen, S. S. Hodgman, M. Schreiber, I. Bloch, and U. Schneider, arXiv:1509.00478.
[63] D. Pekker and B. K. Clark, arXiv:1410.2224.
[64] V. Khemani, F. Pollmann, and S. L. Sondhi, arXiv:1509.00483.
[65] X. Yu, D. Pekker, and B. K. Clark, arXiv:1509.01244.
[66] D. Pekker and B. K. Clark, arXiv:1410.2224.
[67] M. Friesdorf, A. H. Werner, W. Brown, V. B. Scholz, and J. Eisert, Phys. Rev. Lett. **114**, 170505 (2015).
[68] F. Pollmann, V. Khemani, J. I. Cirac, and S. L. Sondhi, arXiv:1506.07179.
[69] A. Chandran, I. H. Kim, G. Vidal, and D. A. Abanin, Phys. Rev. B **91**, 085425 (2015).
[70] T. Devakul and R. R. P. Singh, Phys. Rev. Lett. **115**, 187201 (2015).
[71] R. Vosk, D. A. Huse, and E. Altman, Phys. Rev. X **5**, 031032 (2015).
[72] W. de Roeck, F. Huveneers, M. Müller, and M. Schiulaz, arXiv:1506.01505.
[73] I. Mondragon-Shem, A. Pal, T. L. Hughes, and C. R. Laumann, Phys. Rev. B **92**, 064203 (2015).

[74] X. Wan, D. N. Sheng, E. H. Rezayi, K. Yang, R. N. Bhatt, and F. D. M. Haldane, Phys. Rev. B **72**, 075325 (2005).
[75] D. N. Sheng, X. Wan, E. H. Rezayi, K. Yang, R. N. Bhatt, and F. D. M. Haldane, Phys. Rev. Lett. **90**, 256802 (2003).
[76] L. Sheng, D. N. Sheng, F. D. M. Haldane, and L. Balents, Phys. Rev. Lett. **99**, 196802 (2007).
[77] Y. Y. Atas, E. Bogomolny, O. Giraud, and G. Roux, Phys. Rev. Lett. **110**, 084101 (2013).
[78] M. L. Mehta, *Random Matrices* (Academic, Boston, 1991).
[79] H. F. Song, S. Rachel, C. Flindt, I. Klich, N. Laflorencie, and K. Le Hur, Phys. Rev. B **85**, 035409 (2012).
[80] S. P. Lim and D. N. Sheng, arXiv:1510.08145